Research Square

Preprints are preliminary reports that have not undergone peer review.
They should not be considered conclusive, used to inform clinical practice,
or referenced by the media as validated information.

Senomorphic Suppression of Trypanosoma cruzi-Induced Cellular Senescence

Gauri Naik
Binghamton University
Noah Patric Walsh
Binghamton University
Princess Pokharel
Binghamton University
Jaya Mahendra Singh
Binghamton University
Denisse Martinez
Binghamton University
Raisa Ahmed
Binghamton University
Jacob Aronov
Binghamton University
Azadeh Nasuhidehnavi
anasuhi@binghamton.edu

Binghamton University

Research Article

Keywords: Senescence, Trypanosoma cruzi, senomorphics, metabolism, resveratrol, Chagas disease

Posted Date: November 23rd, 2026

DOI: https://doi.org/10.21203/rs.3.rs-11598789/v1

License: This work is licensed under a Creative Commons Attribution 4.0 International License.
Read Full License

Additional Declarations: No competing interests reported.

Senomorphic Suppression of *Trypanosoma cruzi*-Induced Cellular Senescence

Gauri Naik[1], Noah Patric Walsh[2,3], Princess Pokharel[2], Jaya Mahendra Singh[1], Denisse Martinez[2], Raisa Ahmed[4], Jacob Aronov[2], Azadeh Nasuhidehnavi*[1]

[1] Department of Pharmaceutical Sciences, Binghamton University, Binghamton, New York, USA

[2] Department of Biology, Binghamton University, Binghamton, New York, USA

[3] Binghamton Biofilms Research Center, Binghamton University, Binghamton, New York, USA

[4] Department of Biochemistry, Binghamton University, Binghamton, New York, USA

* Corresponding author:

Azadeh Nasuhidehnavi, PhD, DVM

Department of Pharmaceutical Sciences

Binghamton University School of Pharmacy and Pharmaceutical Sciences

PO Box 6000, Binghamton, NY 13902-6000

Phone: 607-777-5866

anasuhi@binghamton.edu

Keywords: Senescence, Trypanosoma cruzi, senomorphics, metabolism, resveratrol, Chagas disease

Abstract

Trypanosoma cruzi, the causative agent of Chagas disease (CD), induces host cell senescence and metabolic reprogramming that sustain inflammation and tissue damage. Senomorphics suppress senescence-associated phenotypes without eliminating senescent cells, but their effects on infection-induced senescence and metabolic alterations remain unknown. We infected murine C2C12 myoblasts with the *T. cruzi* Brazil strain and evaluated the effects of the senomorphic agent resveratrol. Infection increased senescence-associated markers (p21 and p53), inflammatory and senescence-associated secretory phenotype (SASP) factors (TNF-α, CCL5, and CCL7), the muscle remodeling marker Ankrd1, and senescence-associated β-galactosidase activity. Resveratrol treatment attenuated β-galactosidase activity and reduced p21 and p53 expression induced by *T. cruzi* infection. In addition, untargeted metabolomics revealed infection-associated alterations in intracellular and extracellular lipids, amino acids, peptides, and carbohydrates. Resveratrol enhanced early metabolic responses but reduced intracellular metabolic divergence at later time points and reversed or attenuated changes in selected lipid-, peptide-, and amino acid-related features. These findings indicate that resveratrol mitigates the senescence-like phenotype and modulates infection-associated metabolic remodeling, highlighting its potential as a host-directed strategy to alleviate *T. cruzi*-induced cellular dysfunction.

Introduction

Trypanosoma cruzi, the causative agent of Chagas disease (CD), is an intracellular protozoan parasite that establishes chronic infection in hosts[1]. An estimated 6 million people are infected with *T. cruzi* worldwide, approximately one-third of whom develop serious complications, including chronic cardiomyopathy [2]. CD, historically considered endemic to South and Central America, has emerged as a growing public health concern in the United States [3]. Furthermore, migration has contributed to its globalization, making CD a global health issue [4]. The progression of CD results from a complex interplay between persistent *T. cruzi* infection and sustained host immune responses. Chronic Chagas cardiomyopathy is a multifactorial process driven by the interplay between parasite persistence and host immune responses. Persistent immune stimulation promotes chronic low-grade inflammation and immune-mediated myocardial injury, while continued parasite presence sustains the inflammatory response. Progressive myocardial damage therefore likely results from the combined, and potentially mutually reinforcing, effects of parasite persistence and immune dysregulation [5]. Therefore, understanding host-parasite interactions and the pathways driving chronic inflammation and tissue damage is essential for identifying therapeutic targets to mitigate disease progression

Cellular senescence, a fundamental pillar of aging, is a state in which cells are irreversibly arrested in the cell cycle. A variety of stressors such as telomere attrition, DNA damage, mitochondrial dysfunction, and metabolic dysregulation can induce cellular senescence. This process induces a senescence-associated secretory phenotype (SASP), characterized by the increased production and secretion of inflammatory cytokines and chemokines by senescent cells [6]. In addition, senescent cells exhibit prolonged viability

and resistance to apoptosis, while they possess alterations in metabolic activity compared with non-senecent cells [7]. Recent evidence suggests a role for infection in inducing cellular senescence in host cells by bacteria, viruses, and parasites [7]. In particular, protozoan parasites like *T. cruzi* have evolved sophisticated strategies to manipulate host-cell signaling, metabolism, immune responses, and cellular survival to establish and maintain infection [8,9]. Beyond its direct cytopathic effects, *T. cruzi* actively drives host cells into premature senescence, and this infection-induced senescence is emerging as an independent contributor to CD pathology. Mechanistically, parasite invasion triggers oxidative stress and reactive oxygen species (ROS) production that inflict DNA lesions within the first hour of infection in human cells, including cardiomyocytes [10]. ROS production can induce a senescent state marked by senescence-associated β-galactosidase activity and SASP production[11]. In experimental CD models, this premature senescence phenotype in cardiomyocytes tracks directly with microstructural damage and contractile dysfunction both *in vitro* and *in vivo* [12]. Senescent cells are not inert bystanders and remain metabolically active and exhibit SASP by producing inflammatory mediators like TNF-α, IL-1β, IL-6, and ROS, which may propagate DNA damage and senescence to neighboring cells while sustaining chronic inflammation in cardiac tissue[13]. Early benznidazole treatment attenuated contractile deterioration[14]; however, data from BENEFIT trial showed that parasite clearance once the chronic cardiomyopathy is established is not effective for alleviating cardiac complications[15]. Preventing or reversing infection-induced senescence offers therapeutic potential on grounds independent of parasite killing. Therefore, identifying senescence as a modifiable disease axis, and senolytic or senomorphic strategies that selectively eliminate senescent cells or suppress

the SASP could break the self-amplifying cycle of oxidative damage, inflammation, and progressive cardiac dysfunction that defines chronic Chagas cardiomyopathy.

In chronic infections, prolonged cellular stress and accumulation of senescent cells could contribute to persistent inflammation and tissue dysfunction[16]. Resveratrol, a naturally occurring polyphenolic compound, shows senomorphic potential by modulating senescence-associated pathways, including sirtuin 1, AMPK, and NF-κB signaling[17,18]. Resveratrol has been reported to reduce markers of cellular senescence and suppress the production of pro-inflammatory SASP factors in senescent cells [19,20]. Thus, resveratrol and other senomorphic compounds may offer a complementary strategy for mitigating the detrimental effects of cellular senescence while preserving cell viability. In the context of parasitic infections such as *T. cruzi*, investigating whether resveratrol can modulate infection-associated senescence and inflammation may provide valuable insights into potential host-directed therapeutic strategies.

Senescent cell metabolites and metabolism also significantly differ from non-senescent cells. Some pathways that are altered in healthy, senescent, and infection models include lipids, amino acids, and nucleotides[21–24]. Lipid metabolism changes include but are not limited to sphingomyelin-ceramide and phospholipid pathways[21]. The sphingomyelin-ceramide pathway involves sphingomyelinase (SMase), which hydrolyzes sphingomyelins into phosphocholine and ceramides and is significantly more active in senescent cells[21,25]. SMase activity increases during aging and cellular senescence, elevating ceramide levels in cell types, including fibroblasts and endothelial cells[26,27]. Ceramides exert antiproliferative effects and regulate signal transduction, apoptosis, and growth [28]. Altered ceramide levels may also influence parasitic infections; in *Leishmania*

donovani–infected BALB/c macrophages, increased ceramide synthesis suppressed nitric oxide production and enhanced intracellular parasite survival [29]. Parasite infection also mirrors traits depicted by senescent cells and may contribute to or accelerate host senescence[30]. Therefore, utilizing metabolomics to evaluate metabolic changes in *T. cruzi* infection can offer in-depth temporal snapshots of cellular pathology and potentially novel, druggable targets to modulate or alter senescence and senescent-like phenotypes.

In this study, we investigated whether *T. cruzi* infection induces a senescence-like phenotype accompanied by metabolic dysregulation and whether resveratrol can mitigate these alterations. Our results demonstrated increased expression of senescence-associated markers and disruption of multiple metabolic pathways in *T. cruzi*-infected cells. Resveratrol treatment attenuated the expression of these markers and improved the overall metabolic profile of host cells. These findings provide new insights into the interplay between infection-induced cellular senescence and metabolic dysfunction and highlight resveratrol as a potential strategy for mitigating *T. cruzi*-induced host cell damage.

Materials and Methods

Chemicals

Resveratrol (MPBio, Cat# 0219605205) was dissolved in DMSO or ethanol and diluted in cell culture medium to achieve final concentrations of 5 μM and 40 μM. The final concentration of DMSO or ethanol in the culture medium was maintained at 0.1% (v/v) for all resveratrol treatments and corresponding vehicle controls. Anti-Ssp4 (Amastigote

Surface Antigen) antibody was acquired from BEI Resources, NIAID, NIH (Cat# NR-50892).

Mouse C2C12 Cell and Parasite Culture. Murine C2C12 (American Type Culture Collection, ATCC) and tissue culture-derived *T. cruzi* trypomastigotes, strain Brazil+luc (BEI Resources, NIAID, NIH, Cat#NR-40347) were cultured in 5% CO_2 at 37°C in Dulbecco's Modified Eagle Medium (DMEM) F-12 (Cytiva, Cat# SH30261.01). The media were supplemented with 10% heat-inactivated fetal bovine serum (FBS, Cytiva, Cat# SH3039603), 100 IU/mL of penicillin, and 100 IU/mL of streptomycin (Gibco, Cat# 15070063) and changed every 48 h. All experiments were conducted under biosafety level 2 conditions.

C2C12 Parasite Infection. C2C12 cells, passage 4-10, were seeded at 4×10^4 cells/cm^2 and monitored daily until they reached 80% confluency, typically within approximately 4-5 days. Cells were subsequently infected with trypomastigotes at a multiplicity of infection (MOI) of 5. After 5 hours, C2C12 cells were extensively washed with phosphate-buffered saline (PBS) to remove extracellular parasites and supplemented with DMEM F-12 (10% FBS) for 4h, 24h and 48h.

Fluorescence-Based Microscopy

For fluorescence microscopy, C2C12 cells were plated in Lab-Tek chambers (Thermo Scientific, Cat#154543) and infected with *T. cruzi* trypomastigotes at an MOI of 5 for 24 h and 48 h, as described above. At each timepoint, the cells were fixed with 4% formaldehyde in PBS for 10 min at 37 °C. The cells were then washed with PBS and permeabilized with cold acetone for 4 min. Non-specific binding sites were blocked for 30 min with 3% bovine serum albumin in PBS. Cells were subsequently incubated with the

anti-*T. cruzi* SSP4 antibody (1:200) for 1 h. Following incubation, the cells were washed with PBS and incubated for 30 min with an Alexa Fluor 568-conjugated anti-mouse secondary antibody (1:1000) diluted in blocking buffer. Coverslips were mounted onto microscope slides using ProLong Diamond antifade with DAPI mounting medium (Molecular Probes Cat#P36962). Fluorescence images were acquired using a Keyence BZ-X microscope. The percentage of *T. cruzi*-infected C2C12 cells was determined by counting the number of parasites in three independent chambers from three experiments, with at least 200 cells counted per field. Cells displaying SSP4-positive parasites were considered infected. The infection rate was calculated as the number of parasites divided by the total number of cells counted, then multiplied by 100.

RNA extraction and qRT-PCR assay. C2C12 cells were infected with Brazil+luc trypomastigotes (MOI=5) as described above. Total RNA was isolated using Zymo Research Quick DNA/RNA Miniprep Plus kit (Cat# D7003) or Trizol Reagent (Invitrogen, Cat#15596026) according to the manufacturer's instructions. qRT-PCR was performed using the universal SYBR Green Supermix (Fisherbrand #A59529) on a Bio-Rad CFX-96 Real-Time System. Primer sequences used in the study: p21 F: CGAGAACGGTGGAACTTTGAC, p21R: CAGGGCTCAGGTAGACCTTG. p53 F: CAGCGTGGTACCTTATG, p53 R: AGGTTCCCACTGGAGTCTT. TNF-α F: CCCTCACACTCAGATCATCTTCT, TNF-α R: GCTACGACGTGGGCTACAG. CCL5 F: AGATCTCTGCAGCTGCCCTCA, CCL5 R: GGAGCACTTGCTGCTGGTGTAG. CCL7 F: AAGATCCCCAAGAGGAATCTCAAG, CCL7 R: CAGACTTCCATGCCCTTCTTTG. Ankrd-1 F: GCTGGAGCCCAGATTGAA, Ankrd-1 R: CTCCACGACATGCCCAGT. Gata4 F: CTGGAAGACACCCCAATCTC, Gata4 R: GTAGTGTCCCGTCCCATCTC. gadd45g F: GCGAGGCAGGTGTGACTC, gadd45g R: CCTTTCTTTCCCCTCCTTTCA. 18s F: ACTCAACACGGGAAACCTCAC, 18s R: CATGCCAGAGTCTCGTTCGTT. Aldoa F:

ATACTCCCTCGGCCCTGG, Aldoa R: CATCAGGGAGAATTTCAGGCTC. Relative mRNA expression was normalized to 18S and Aldoa, which were used as reference genes

Senescence-associated β-galactosidase assay

C2C12 cells were infected with Brazil+luc trypomastigotes (MOI=5) as described above. For treatment experiments, cells were treated with resveratrol 5 μM or 40 μM or vehicle (DMSO) for 24 h. SA-β-Gal staining was performed using the Senescence β-Galactosidase Staining kit (Cell Signaling Technology, Cat#9860). Briefly, cells were washed with PBS and fixed with 1X fixative reagent for 10 min at room temperature. Then, cells were washed with PBS and stained with β-Galactosidase staining solution at pH 6.0 and kept in a 37 °C incubator without CO2 overnight. The staining solution was removed, and cells were rinsed with PBS. For quantification, phase-contrast images were captured using an Olympus DP80 microscope. Blue-stained C2C12 cells and the total number of cells were counted, and data were plotted as the percentage of SA-β-Gal-positive cells/total number of cells in each field.

Cell viability assay

C2C12 cells were seeded into a 96-well plate at a density of 500 cells per well and incubated for 24 h prior to treatment with resveratrol. The cells were incubated with a range of resveratrol concentrations from 800 μM to 2.5 μM for 24 h and 48 h. After each timepoint, cell viability was assessed using an MTS assay kit (Promega, Cat#65421) based on the manufacturer's instructions. Briefly, 20 μL of MTS+PMS reagent was added to each well. Following 1 h of incubation in a 37 °C incubator with 5% CO2, the absorbance at 490 nm of each well was measured by the Varioskan LUX multimode microplate reader (ThermoFisher).

Metabolite extraction and LC-MS/MS data collection

Both intracellular and extracellular (media) metabolites were collected from samples. At least one 1 mL of media was collected from samples in 1.5-mL Eppendorf tubes and kept on ice. Remaining media was discarded, and the cells were washed with 3 mL of phosphate-buffered saline (PBS). Cells were then detached from plates by adding 0.5 mL of trypsin enzyme and incubating at 37° C, then 1 mL of fresh medium was added to dilute trypsin. The cell suspension was then added to a 2-mL screw-cap tube and centrifuged at 300 x g at 4° C for five minutes. The supernatant was discarded, and the cell pellet was washed with 1 mL of LC-MS grade water to remove excess media. After washing, 100 µL of zirconia-silica beads (BioSpec, Cat# 11079105z) were added to the samples along with 200 µL of a 1:1 part 100% LC-MS grade methanol and water buffer spiked with 2 µM sulfachloropyridazine. Samples were then homogenized in a Precellys Evolution Touch Homogenizer for 15 seconds at 5,500 rpm with one 30-second rest period for two cycles. Samples were centrifuged at 4°C for 10 minutes at 16,000 x g. After centrifugation, the supernatant was collected, henceforth referred to as the aqueous extract. The above process was then repeated to the aqueous extract pellet with the addition of 200 µL of a 3:1 parts LC-MS grade dichloromethane (DCM) and 100% methanol buffer spiked with 2 µM of sulfachloropyridazine. The supernatant collected from extraction with DCM: methanol is referred to as the organic extract.

Extracellular metabolite collection was adapted from a previous study[31]. 1 mL of collected culture media was spun down at 1,000 x g for 5 minutes. 100 µL of the topmost portion of the supernatant was transferred to a new 1.5-mL Eppendorf tube, and 900 µL of a 3:1 parts acetonitrile to 100% methanol solution spiked with 2 µM sulfachloropyridazine was

added to the tube and vortexed. The sample was then spun down at 18,000 x g in a 4°C centrifuge for 10 minutes. The topmost 200 µL was collected for further analysis. Aqueous and extracellular extracts were dried in a SpeedVac overnight, and organic extracts were left to air-dry in the fume hood. Both fractions were collected the next day and stored in a -80°C freezer prior to resuspension.

Aqueous and organic extracts were resuspended for LC-MS analysis with 120 µL of 1:1 part 100% methanol and LC-MS grade water buffer, spiked with 2 µM of sulfadimethoxine as an internal standard. The extracts were combined and samples sonicated for 10 minutes, centrifuged at 10,000 x g for 4 minutes in 4°C pre-chilled centrifuge, and supernatants transferred to new 1.5-mL Eppendorf tubes. Centrifugation was repeated, and supernatant was transferred to new 1.5-mL Eppendorf tubes. A quality control (QC) sample was created by adding 5 uL of each sample within a group to a new tube. Prior to running samples, two blanks then a solution with 6 known molecules were run to determine instrument shift. Between each experimental group, blanks and QCs were run to condition the column, and samples were randomized within groups. Spectra were checked during runs to ensure no peak shift. A Bruker TimsTOF Pro2 mass spectrometer coupled with nanoElute 2 nano-LC was used to analyze samples using an Acquity Premier BEH C18 VanGuard FIT column (Waters, Part# 186009457) and Acquity Premier BEH C18 VanGuard FIT cartridge (Waters, Part# 186009459). Chromatography was done with water with 0.1% formic acid (mobile phase A) and acetonitrile with 0.1% formic acid (mobile phase B), at a 0.3 mL/min flow rate with a 40-degree Celsius column temperature. LC gradient for the sample for mobile phase A is as follows: 0-1 min, hold at 98% A; 1-6 min, decrease A to 0%; 6-9 min, hold at 0% A; 9-9.1 min, increase to 98%

A; 9.1-12 min, hold at 98% A. LC gradient for mobile phase B is as follows: 0-1 min, hold at 2% B; 1-6 min, increase B from 2% to 100%; 6-9 min, hold B at 100%; 9-9.1 min, decrease B from 100% to 2%; 9.1-12 min, hold B at 2%. 0-1 min, hold at 98% A and 2% B; 1-6 min, hold at 100% B; 9-9.1 min, increase A to 98% and decrease B to 2%; 9.1-12 min, hold at 98% A and 2% B.

MS instrument parameters were as follows: runtime: 0 to 12 minutes; polarity: positive; nebulizer gas pressure: 2.2 bar; capillary voltage: 4500 V; ion source temperature: 220°C; dry gas flow: 9 l/min; spectra acquisition rate: 4 Hz; mass range: 20-1,300 m/z; active exclusion: 0.1 min. The stepping-enabled method has two collision energies: 20 eV and 50eV.

Metabolomics data analysis

Data collected were processed in Metaboscape with the processing parameters as described in Supplementary Table 1.

Metaboscape data were loaded into R (version 4.5.2) for data tidying, with an m/z tolerance of 0.0005 and a retention time tolerance of 15 seconds. Removal of overlapping peaks and features that did not exceed blanks by the specified threshold was performed, and the resulting output was normalized by total ion current (TIC). Normalized data were uploaded for feature-based molecular networking (FBMN) in the Global Natural Products Social Molecular Networking (GNPS) [32,33]. Chemical families were assigned to compounds with both SMILES and compound names using NPClassifier (from package chemodiv version 0.3.1) [34]. Compounds whose annotations were not available through GNPS2, NPClassifier, or Cytoscape (version 3.10.4) were excluded from downstream

data exploration and visualization. Bar charts of chemical families for experimental groups were generated using ggplot2 (version 4.0.2). Box plots of individual metabolites were generated in Python (version 3.14.3) and packages pandas (version 3.0.1), numpy (version 2.4.2), matplotlib (version 3.10.8), seaborn (version 0.13.2), statannotations (version 0.7.2), statsmodels (version 0.14.6).

Principal coordinates analysis (PCoA) was performed on TIC-normalized data using the Bray-Curtis and Faith's phylogenetic dissimilarity metrics in QIIME2 [35]. PCoA plots were visualized in Emperor [36].

Statistical analysis

Wilcox tests were performed for each metabolite using the wilcox.test() function from the *stats* package in R (version 4.5.2), and a list of significant metabolites for each sample group was generated. Adjusted p-values were calculated using the p.adjust() function with the "fdr" method. Fold changes were calculated as infected groups over uninfected groups for all metabolites. The lists were then filtered down to metabolites with a p-adjusted value of less than 0.05; all downstream analyses were carried out with metabolites with a p-adjusted value of less than 0.05.

Results

Characterization of *T. cruzi* Infection in C2C12 cells

C2C12 murine myoblasts are permissive to infection with multiple *T. cruzi* strains and mount a robust inflammatory response upon infection[37,38]. As an initial characterization step, we evaluated the infectivity of the *T. cruzi* Brazil strain in C2C12 cells at MOI of 5. Cells were seeded onto chamber slides and exposed to tissue culture-derived trypomastigotes for 5 hours to allow parasite entry, after which the culture medium was replaced to remove extracellular parasites. Infected cultures were then maintained for an additional 24 h or 48 h. Infection rates were quantified by immunostaining for SSP4, a marker specific to the intracellular amastigote stage of *T. cruzi*, revealing infection rates of 8.06% and 25.23% at 24 and 48 h post-infection, respectively (**Fig. 1A-B**). Taken together, our results showed that *T. cruzi* Brazil strain productively infects C2C12 myoblasts, confirming this system as a suitable *in vitro* model for studying the progression of host-parasite interactions during *T. cruzi* infection.

T. cruzi induces senescence-like phenotype in C2C12 cells

We next asked whether *T. cruzi* infection drives host cells toward a senescence-like phenotype, as has been reported in other cell types. Several studies have shown that *T. cruzi* infection induces a senescence-like phenotype in host cells [11,39]. Consistent with these findings, we observed that infection of C2C12 myoblasts led to early activation of canonical cell cycle arrest pathways, evidenced by increased expression of the senescence-associated regulators p21 and p53 (**Fig. 2A**). In parallel, *T. cruzi* infection elicited upregulation of several components of SASP factors, including the pro-inflammatory cytokine tumor necrosis factor-α (TNF-α). Moreover, age-associated chemokines implicated in chronic inflammation and tissue remodeling, such as CCL5 and CCL7, were significantly elevated in infected cells (**Fig. 2B**).

Given that cellular senescence is also characterized by pronounced morphological and structural remodeling, and *T. cruzi* infection has been shown to alter host cell structure [39], we next examined markers associated with hypertrophic and stress-responsive programs. Notably, expression of ankyrin repeat domain-containing protein 1 (Ankrd1), a mechanosensitive marker linked to muscle remodeling, was markedly increased following infection (**Fig. 2C**). In addition, we observed upward trends in other senescence- and aging-related regulators, including GATA binding protein 4 (GATA4) and growth arrest and DNA damage-inducible protein 45 (GADD45) (**Fig. 2C**), further supporting the induction of a senescence-like state in *T. cruzi*-infected C2C12 cells.

To functionally validate the senescence-like phenotype suggested by our gene expression data, we assessed senescence-associated β-galactosidase (SA-β-gal) activity using the SA-β-gal staining assay, a widely used and well-established marker of cellular senescence[40]. Consistent with the upregulation of p21, p53, and SASP components observed at earlier time points, SA-β-gal activity was increased by 2.27-fold in *T. cruzi*-infected C2C12 cells at 24 hours post-infection compared to uninfected controls (**Fig. 2D**). Because SA-β-gal positivity reflects an accumulation of senescence-associated lysosomal changes rather than a single molecular pathway, this finding provides functional confirmation that *T. cruzi* infection drives host cells toward a senescent phenotype, rather than merely inducing transient stress-response gene expression.

Resveratrol, a senomorphic agent, attenuates *T. cruzi*-induced host cell senescence

Resveratrol has been widely reported to mitigate cellular senescence across diverse pathological contexts, including cigarette smoke-induced senescence in skeletal muscle [41], high-fat diet-associated senescence in aortic endothelial cells[42], and replicative senescent human fibroblasts[43]. Despite these established anti-senescent effects, the potential role of resveratrol in modulating host cell aging responses during *T. cruzi* infection has not been previously investigated. To address this gap, we examined the impact of resveratrol treatment on *T. cruzi*-infected C2C12 myoblasts.

We first evaluated the cytotoxicity of resveratrol in C2C12 myoblasts and *T. cruzi* trypomastigotes using a range of concentrations between 5-800 μM. Previous studies have demonstrated that resveratrol at a concentration of 5 μM remains approximately 75% stable in culture medium after 48 hours of incubation [43], supporting its suitability for *in vitro* experiments. We observed C2C12 cell viability remained above 1 compared to untreated cells in concentrations below 100 μM following 48 h of treatment, indicating that these doses were non-toxic under our experimental conditions (**Supplementary Fig. 1 A-B**). We selected 5 and 40 μM resveratrol to evaluate its senomorphic effects. Resveratrol at 5 μM significantly attenuated *T. cruzi*-induced SA-β-gal activity, restoring levels comparable to uninfected controls, whereas the higher concentration (40 μM) was less effective (**Fig. 3A-B**). 5 μM resveratrol treatment also decreased levels of infection-induced p21 and p53 at 48 h post-infection by approximately 77% and 72%, respectively **(Fig. 3C-D)**. Collectively, these results indicate a senomorphic effect of resveratrol during *T. cruzi* infection, underscoring its potential to modulate host aging-associated pathways without compromising cell viability.

Resveratrol ameliorates *T. cruzi*-induced metabolic perturbations

Given the importance of metabolism in aging and resveratrol metabolic effects, we assessed how infection and resveratrol treatment (5 μM) affected overall small-molecule profiles between infected and uninfected groups. To provide a more detailed picture, we analyzed intracellular and extracellular metabolites separately using PERMANOVA. The results revealed that intracellular metabolome of infected and uninfected groups in vehicle and resveratrol treatment were significantly different at both 24 h and 48 h post-infection (**Fig. 4A-B, Supplementary Table 2**). Distance analysis revealed that in the ethanol (vehicle) control, the metabolic difference of intracellular metabolites between infected and uninfected cells increased over time, from a pseudo-F of 5.03 at 24 h (PERMANOVA, Bray-Curtis; p-value = 0.004, 999 permutations, n = 16 samples, 2 groups) to a pseudo-F of 8.45 at 48 h (PERMANOVA, Bray-Curtis; p-value = 0.002, 999 permutations, n = 16 samples, 2 groups) (**Fig. 4C-D, Supplementary Table 2**), indicating a growing metabolic divergence as infection progressed. In contrast, resveratrol treatment produced the strongest separation at 24 h (PERMANOVA, Bray-Curtis; pseudo-F = 10.34, p-value = 0.001, 999 permutations, n = 16 samples, 2 groups), which exceeded that of the ethanol control at the same time point (**Fig. 4C-D, Supplementary Table 2**). This suggests that resveratrol amplified the early metabolic response of infected cells. By 48 h, however, the infected versus uninfected difference in resveratrol-treated cells had decreased markedly (PERMANOVA, Bray-Curtis; pseudo-F = 3.47, p-value = 0.002, 999 permutations, n = 16 samples, 2 groups) and was well below the ethanol control at 48 h (**Fig. 4C-D, Supplementary Table 2**). Direct comparison of infected cells (vehicle vs resveratrol) confirmed that resveratrol significantly altered the intracellular metabolome at both time points, although the effect weakened over time (PERMANOVA, Bray-Curtis; 999

permutations, n = 16 samples, 2 groups, 24 h: pseudo-F = 4.82, p-value = 0.001; 48 h: pseudo-F = 2.72, p-value = 0.001; **Supplementary Table 2**). Collectively, these findings indicate that resveratrol alters the temporal dynamics of the host metabolic response to *T. cruzi* infection. While infection progressively increased metabolic divergence in vehicle-treated cells, resveratrol amplified the early response at 24 h and attenuated this divergence by 48 h. Thus, resveratrol appears to promote an early metabolic perturbation followed by partial metabolic normalization during infection.

PERMANOVA analysis of extracellular metabolite profiles showed that *T. cruzi* infection significantly altered the overall metabolome under both treatments at 24 h post-infection, and resveratrol altered this pattern at 48 h post-infection (**Fig.5 A-B, Supplementary Table 3**). In the ethanol (vehicle) control, infected and uninfected cells differed modestly at 24 h (PERMANOVA, Bray-Curtis; pseudo-F = 1.997, p-value = 0.048, 999 permutations, n = 16 samples, 2 groups), and the difference was similar at 48 h (PERMANOVA, Bray-Curtis; pseudo-F = 2.478, p-value = 0.026, 999 permutations, n = 16 samples, 2 groups) (**Fig.5 C-D, Supplementary Table 3**). In resveratrol-treated cells, the infected versus uninfected difference was strongest at 24 h (PERMANOVA, Bray-Curtis; pseudo-F = 3.677, p-value = 0.003, 999 permutations, n = 16 samples, 2 groups), exceeding that of the ethanol control, which suggests that resveratrol amplified the early extracellular response to infection. By 48 h, this difference had decreased (pseudo-F = 2.462, q-value = 0.007) and was comparable to the ethanol control, suggesting that resveratrol can alleviate the infection-associated metabolic perturbations at 48 h relative to its own 24 h profile (**Fig.5 C-D, Supplementary Table 3**). In contrast, the difference between the two infected groups increased over time. At 24 h, infected ethanol and

infected resveratrol cells did not differ significantly (PERMANOVA, Bray-Curtis; pseudo-F = 1.591, p-value = 0.06, 999 permutations, n = 16 samples, 2 groups), whereas at 48 h they were clearly separated (PERMANOVA, Bray-Curtis; pseudo-F = 2.928, p-value = 0.021, 999 permutations, n = 16 samples, 2 groups) (**Supplementary Table 3**). This indicates that resveratrol progressively reshaped the extracellular metabolite profile of infected cells, with the treatment effect becoming significant only at the later time point.

Resveratrol modifies infection-associated metabolic changes in *T. cruzi*-infected cells

To identify individual metabolites impacted by *T. cruzi* infection and resveratrol treatment, p-values were calculated by comparing each infected group with its time- and treatment-matched uninfected control (vehicle-treated infected vs. vehicle-treated uninfected, and resveratrol-treated infected vs. resveratrol-treated uninfected, at 24 and 48 h post-infection). The resulting p-values were then adjusted for the false-discovery rate (FDR). Fold change values for each condition were calculated by dividing the mean TIC-normalized signal intensity of the metabolite in the infected group by the mean TIC-normalized signal intensity of the same metabolite in the matched uninfected control. Metabolites with an FDR-adjusted p-value < 0.05 were considered significantly altered.

Infection altered multiple metabolite families at 24 and 48 h post-infection, including lipids and lipid-like molecules, amino acids and peptides, carbohydrates, and alkaloids (**Fig. 6A-D**). Lipids, including glycerophosphocholines, fatty amides, and sphingolipids, contained the largest number of significantly altered features between uninfected and infected groups at both time points (FDR < 0.05), followed by amino acids and peptides.

Among the features that differed by infection, lysophosphatidylcholine (18:3) (m/z 517.3165 RT 363.68 sec) was higher in infected cells at 24 h post-infection, lower in infected cells treated with resveratrol than in vehicle-treated infected cells (**Fig. 7A**). Similarly, an intracellular peptide-like feature (m/z 375.219 RT 198.46 sec) increased with infection at 24 h and was reduced by resveratrol (**Fig. 7B)**. Extracellular phenylalanine (m/z 165.0788 RT 61.42 sec) decreased at 48 h post-infection, resveratrol treatment significantly increased phenylalanine levels in infected cells (**Fig. 7C**). These results suggest that resveratrol is associated with changes in specific lipid, and amino acid features during infection. Whether these changes reflect direct effects on host metabolism, reduced parasite burden, or both was not determined in this study.

Discussion

In this study, we demonstrated that *T. cruzi* infection of C2C12 myoblasts induces a senescence-like phenotype characterized by activation of the p53/p21 axis, development of SASP-associated profile, and increased SA-β-gal activity. These cellular changes are accompanied by progressive, time-dependent remodeling of both the intracellular and extracellular metabolomes. Resveratrol, administered at a non-cytotoxic concentration, attenuated senescence-associated markers and modulated the metabolic response, enhancing early metabolic perturbations at 24 h while partially restoring metabolic homeostasis by 48 h. Collectively, these findings identify infection-induced senescence-like alterations and their associated metabolic remodeling as modifiable components of the host response to *T. cruzi* infection and support the potential of resveratrol as a senomorphic agent capable of modulating this response.

Our findings demonstrate that *T. cruzi* infection induces a senescence-like phenotype in skeletal muscle cells, extending previous observations of *T.cruzi*-associated cellular senescence in other host cell types[11,39]. In cardiomyocytes, *T. cruzi*-induced premature senescence has been linked to contractile dysfunction both *in vitro* and *in vivo*. The attenuation of this phenotype following early antiparasitic treatment further suggests that senescence may contribute to CD pathology beyond being a consequence of infection[39]. Our findings are consistent with this possibility. In infected myoblasts, we observed increased expression of p53 and its downstream cyclin-dependent kinase inhibitor p21, together with elevated SA-β-gal activity. In addition, increased expression of SASP-associated components, including TNF-α and the chemokines CCL5 and CCL7, which are secreted by senescent cells and can recruit and activate innate and adaptive immune cells such as monocytes/macrophages, NK cells and T cells[44,45], suggests that infected myoblasts acquire a pro-inflammatory secretory phenotype. Because these mediators can also be induced by innate immune recognition of the parasite [46,47], their expression alone is insufficient to establish a senescence-associated phenotype. However, in conjunction with p53/p21 activation and increased SA-β-gal activity, their upregulation is consistent with the development of a senescence-associated secretory phenotype that may contribute to persistent local inflammation and leukocyte recruitment in chronically infected skeletal muscle.

Resveratrol attenuated several senescence-associated features in *T. cruzi*-infected cells, supporting its potential role as a senomorphic modulator of the host response to infection. At non-cytotoxic concentrations, resveratrol reduced SA-β-gal activity and decreased p21 and p53 expression. This pattern is consistent with senomorphic effects whereby

senescence-associated phenotypes and potentially their secretory activity are attenuated without evidence of selective elimination of senescent cells [48,49], in contrast to senolytic agents such as dasatinib plus quercetin [50]. However, as we did not directly assess senescent-cell clearance or quantify the SASP following treatment, these findings support a senomorphic interpretation rather than definitively establishing this mechanism.

Mechanistically, resveratrol has been reported to modulate the NAD^+-dependent deacetylase SIRT1[51], which can regulate p53 activity, NF-κB-dependent inflammatory transcription, and mitochondrial function[52]. Although SIRT1 activity and downstream signaling were not directly assessed in our study, this pathway represents a plausible mechanism underlying the observed changes in senescence-associated markers. Further experiments will be needed to determine whether SIRT1 mediates the effects of resveratrol in *T. cruzi*-infected myoblasts.

Notably, 5 μM resveratrol restored SA-β-gal activity to levels comparable to those of uninfected controls, whereas 40 μM produced a less pronounced effect. This non-monotonic response suggests that the effects of resveratrol depend on concentration, consistent with biphasic responses reported in endothelial cells [53], cardiomyocytes [54] , and C2C12 muscle cells [55]. At higher concentrations, resveratrol may exert less favorable effects depending on the cellular context, including changes in redox balance. Our findings highlight the importance of dose optimization when evaluating resveratrol as a modulator of infection-associated cellular senescence and suggest that lower concentrations may be more effective than higher concentrations in *T. cruzi* infection models.

Infection progressively deepened intracellular metabolic divergence in vehicle-treated cells over 48 h, consistent with the extensive host-cell metabolic reprogramming *T. cruzi* imposes to support intracellular replication [8,56]. Consistent with this, *in vivo* untargeted metabolomics show disturbed energy metabolism, with a significantly altered carnitine shuttle and reduced ATP in *T. cruzi*-infected hearts, indicating impaired cardiac metabolic flexibility [57,58]. End-stage human Chagasic myocardium also shows altered acylcarnitines and branched-chain amino acids, along with decreased fatty-acid oxidation [59].

Within this context, the temporal metabolic trajectory observed following resveratrol treatment is particularly informative. Resveratrol was associated with a pronounced increase in the separation between infected and uninfected cells at 24 h, followed by substantial attenuation at 48 h, when resveratrol-treated infected cells were metabolically closer to their uninfected counterparts than were vehicle-treated infected cells to their respective controls. This pattern suggests that resveratrol reshapes the temporal dynamics of the host-cell metabolic response, eliciting an early, amplified perturbation followed by partial normalization, rather than uniformly suppressing infection-associated metabolic changes. The extracellular metabolome exhibited a distinct temporal pattern, characterized by modest infection-associated effects under vehicle treatment, an early peak in the resveratrol response, and a treatment effect in infected cells that was not statistically significant at 24 h but became evident by 48 h. This temporal divergence between intracellular and extracellular compartments may reflect differences in the kinetics with which metabolic changes emerge and are propagated, given that extracellular profiles integrate processes such as metabolite secretion, release, and nutrient consumption over time. Accordingly, intracellular metabolic remodeling may

precede detectable changes in the extracellular milieu. These findings underscore the importance of time-resolved, compartment-specific metabolomic profiling, as analyses restricted to a single time point or metabolic compartment could overlook key features of the resveratrol-associated response.

Lipids dominated the infection-responsive metabolic features, particularly glycerophosphocholines, fatty amides, and sphingolipids. At 24 h, increases in lysophosphatidylcholine (18:3) was reversed by resveratrol, suggesting that treatment modulates infection-associated membrane phospholipid remodeling. Such changes may reflect the substantial demands of intracellular amastigote replication for membrane biogenesis and lipid acquisition. Moreover, lysophosphatidylcholines can act as pro-inflammatory mediators[60], raising the possibility that their accumulation contributes to the inflammatory milieu associated with the SASP. Peptide levels also altered with infection and resveratrol treatment could renormalize them. Among them, extracellular levels of the essential amino acid phenylalanine decreased following infection and were normalized by resveratrol treatment. Although intracellular phenylalanine levels were not measured, these findings suggest that *T. cruzi* infection may increase phenylalanine utilization or catabolism. Further studies are needed to determine how infection affects phenylalanine metabolism in host cells. Interestingly, phenylalanine levels increase with age in mice, accompanied by enhanced phenylalanine catabolism in the heart, which is associated with cardiac dysfunction [62]. Investigating whether altered phenylalanine metabolism contributes to infection-induced cellular senescence may therefore reveal novel therapeutic avenues for CD.

Chronic CD reflects the combined and mutually reinforcing effects of persistent parasitism and host immune-mediated tissue injury [5]. The BENEFIT trial demonstrated that antiparasitic treatment does not necessarily reverse established cardiac disease[15], underscoring the need for complementary host-directed strategies that target the pathological tissue response. Our findings identify infection-induced cellular senescence and its associated metabolic alterations as potential therapeutic targets. Senescent muscle cells may sustain inflammation and tissue remodeling through responding to SASP factors [63], potentially perpetuating pathology beyond the direct effects of parasite persistence. In our model, resveratrol treatment attenuated both senescence-associated markers and infection-associated metabolic divergence, supporting the potential of modulating the senescence-metabolism axis as a host-directed therapeutic approach. Although the clinical utility of resveratrol is constrained by its poor oral bioavailability [64], these findings provide a rationale for investigating other senomorphic agents capable of modulating senescence-associated processes during *T. cruzi* infection, such as the AMPK activator metformin and pterostilbene, resveratrol analogs with substantially greater oral bioavailability [65].

Although our findings provide important insights into the relationship between *T. cruzi* infection, cellular senescence, and metabolic reprogramming, several limitations should be acknowledged when interpreting the results. First, this study used a single murine myoblast cell line and examined responses during the first 48 h of infection. Accordingly, the model captures early host-cell responses rather than the complex pathophysiology of chronic Chagas cardiomyopathy, and the findings require validation in human cardiomyocytes and relevant *in vivo* models. Second, infection rates were relatively

modest, meaning that the metabolomic profiles represent population-level averages encompassing both infected cells and uninfected bystander cells. Although bystander responses may be biologically relevant to paracrine senescence, their inclusion limits the attribution of observed metabolic changes to cell-autonomous responses in infected cells. Third, the present metabolomic analyses cannot distinguish whether the effects of resveratrol arise from direct modulation of host-cell metabolic pathways, reductions in intracellular parasite burden, or a combination of these mechanisms. Future studies incorporating parasite-load-normalized analyses and burden-matched controls will be necessary to disentangle these contributions. Establishing pharmacokinetic-pharmacodynamic relationships *in vivo* and evaluating more bioavailable resveratrol formulations or analogues will therefore be important steps toward assessing the therapeutic potential of targeting infection-associated senescence and metabolic dysregulation in CD.

Conclusion

T. cruzi infection induces a senescence-like phenotype associated with substantial metabolic reprogramming in C2C12 myoblasts. Resveratrol attenuates senescence-associated features while reshaping the temporal dynamics of the host metabolic response, characterized by an early amplification of metabolic perturbations followed by partial normalization. These findings identify infection-associated senescence and metabolic dysregulation as potentially interconnected and therapeutically actionable components of the host response to *T. cruzi*. These results also provide a rationale for evaluating senomorphic strategies *in vivo*, particularly in aging hosts, in whom pre-existing senescent-cell accumulation and impaired metabolic flexibility may exacerbate

infection-associated tissue injury. Further studies are needed to determine whether targeting this senescence-metabolism axis can mitigate tissue pathology and improve disease outcomes in CD.

Declarations

Ethics approval and consent to participate

Not applicable. This study did not involve human participants or animals.

Consent for publication

Not applicable

Availability of data and materials

Metabolomics raw mass spectrometry data have been deposited in the MassIVE repository (https://massive.ucsd.edu) under accession number MSV000103789 and are publicly available at the time of publication at ftp://massive-ftp.ucsd.edu/v15/MSV000103789 at the time of publication. GNPS feature-based molecular network can be accessed at the GNPS link (https://gnps2.org/status?task=49dc9fdc10a84c7aafcdf61c5eaea4c4). All code utilized has been deposited in GitHub (https://github.com/gnaik20/Nasuhidehnavi-Binghamton).

Competing interests

Authors declare no competing interests.

Funding

Not applicable

Authors' contributions

GN, NW, PP, JMS, DM, RA, and JA contributed to data acquisition. GN, NW, and AN contributed to data analysis and interpretation. AN and GN drafted the original manuscript. All authors contributed to reviewing and editing the manuscript. AN supervised the study. All authors read and approved the final manuscript.

Acknowledgements

Not applicable

References

1. Chagas, C. Nova tripanozomiaze humana: estudos sobre a morfolojia e o ciclo evolutivo do Schizotrypanum cruzi n. gen., n. sp., ajente etiolojico de nova entidade morbida do homem. *Mem. Inst. Oswaldo Cruz* **1**, 159–218 (1909).
2. Echeverría, L. E. *et al.* WHF IASC Roadmap on Chagas Disease. *Glob. Heart* **15**, 26 (2020).
3. Beatty, N. L., Hamer, G. L., Moreno-Peniche, B., Mayes, B. & Hamer, S. A. Chagas Disease, an Endemic Disease in the United States. *Emerg. Infect. Dis.* **31**, (2025).
4. Conners, E. E., Vinetz, J. M., Weeks, J. R. & Brouwer, K. C. A global systematic review of Chagas disease prevalence among migrants. *Acta Trop.* **156**, 68–78 (2016).
5. Bonney, K. & Engman, D. Chagas Heart Disease Pathogenesis: One Mechanism or Many? *Curr. Mol. Med.* **8**, 510–518 (2008).
6. Coppé, J.-P., Desprez, P.-Y., Krtolica, A. & Campisi, J. The senescence-associated secretory phenotype: the dark side of tumor suppression. *Annu. Rev. Pathol.* **5**, 99–118 (2010).
7. Di Micco, R., Krizhanovsky, V., Baker, D. & d'Adda Di Fagagna, F. Cellular senescence in ageing: from mechanisms to therapeutic opportunities. *Nat. Rev. Mol. Cell Biol.* **22**, 75–95 (2021).
8. Chiribao, M. L., Libisch, G., Parodi-Talice, A. & Robello, C. Early *Trypanosoma cruzi* Infection Reprograms Human Epithelial Cells. *BioMed Res. Int.* **2014**, 1–12 (2014).
9. Cardoso, M. S., Reis-Cunha, J. L. & Bartholomeu, D. C. Evasion of the Immune Response by Trypanosoma cruzi during Acute Infection. *Front. Immunol.* **6**, (2016).

10. Florentino, P. T. V. *et al.* DNA damage and oxidative stress in human cells infected by Trypanosoma cruzi. *PLOS Pathog.* **17**, e1009502 (2021).

11. Guimarães-Pinto, K. *et al.* Trypanosoma cruzi Infection Induces Cellular Stress Response and Senescence-Like Phenotype in Murine Fibroblasts. *Front. Immunol.* **9**, 1569 (2018).

12. Nogueira, S. S. *et al.* Oxidative stress, cardiomyocytes premature senescence and contractile dysfunction in in vitro and in vivo experimental models of Chagas disease. *Acta Trop.* **244**, 106950 (2023).

13. Guimarães-Pinto, K. *et al.* Cellular Stress and Senescence Induction during Trypanosoma cruzi Infection. *Trop. Med. Infect. Dis.* **7**, 129 (2022).

14. Francisco, A. F., Jayawardhana, S., Taylor, M. C., Lewis, M. D. & Kelly, J. M. Assessing the Effectiveness of Curative Benznidazole Treatment in Preventing Chronic Cardiac Pathology in Experimental Models of Chagas Disease. *Antimicrob. Agents Chemother.* **62**, e00832-18 (2018).

15. Morillo, C. A. *et al.* Randomized Trial of Benznidazole for Chronic Chagas' Cardiomyopathy. *N. Engl. J. Med.* **373**, 1295–1306 (2015).

16. Johnson, A. *et al.* The impacts of chronic infections on shaping cellular senescence. *Immun. Ageing* **22**, 37 (2025).

17. Della Vedova, L., Baron, G., Morazzoni, P., Aldini, G. & Gado, F. The Potential of Polyphenols in Modulating the Cellular Senescence Process: Implications and Mechanism of Action. *Pharmaceuticals* **18**, 138 (2025).

18. Ido, Y. *et al.* Resveratrol prevents oxidative stress-induced senescence and proliferative dysfunction by activating the AMPK-FOXO3 cascade in cultured primary human keratinocytes. *PloS One* **10**, e0115341 (2015).

19. Pitozzi, V. *et al.* Chronic Resveratrol Treatment Ameliorates Cell Adhesion and Mitigates the Inflammatory Phenotype in Senescent Human Fibroblasts. *J. Gerontol. A. Biol. Sci. Med. Sci.* **68**, 371–381 (2013).

20. Chen, H. *et al.* Mesenchymal stem cell-specific Sirt1 overexpression prevents sarcopenia induced by 1,25-dihydroxyvitamin D deficiency. *Aging* https://doi.org/10.18632/aging.206232 (2025) doi:10.18632/aging.206232.

21. Wiley, C. D. & Campisi, J. The metabolic roots of senescence: mechanisms and opportunities for intervention. *Nat. Metab.* **3**, 1290–1301 (2021).

22. Hamsanathan, S. *et al.* A molecular index for biological age identified from the metabolome and senescence-associated secretome in humans. *Aging Cell* **23**, e14104 (2024).

23. Moaddel, R. *et al.* Cross-sectional analysis of healthy individuals across decades: Aging signatures across multiple physiological compartments. *Aging Cell* **23**, e13902 (2024).

24. Ewald, S., Nasuhidehnavi, A., Feng, T.-Y., Lesani, M. & McCall, L.-I. The intersection of host in vivo metabolism and immune responses to infection with kinetoplastid and apicomplexan parasites. *Microbiol. Mol. Biol. Rev. MMBR* **88**, e0016422 (2024).

25. Trayssac, M., Hannun, Y. A. & Obeid, L. M. Role of sphingolipids in senescence: implication in aging and age-related diseases. *J. Clin. Invest.* **128**, 2702–2712 (2018).

690 26. Venable, M. E., Lee, J. Y., Smyth, M. J., Bielawska, A. & Obeid, L. M. Role of
691 Ceramide in Cellular Senescence. *J. Biol. Chem.* **270**, 30701–30708 (1995).
692 27. Venable, M. E. & Yin, X. Ceramide induces endothelial cell senescence. *Cell*
693 *Biochem. Funct.* **27**, 547–551 (2009).
694 28. Obeid, L. M. & Hannun, Y. A. Ceramide: a stress signal and mediator of growth
695 suppression and apoptosis. *J. Cell. Biochem.* **58**, 191–198 (1995).
696 29. Ghosh, S. *et al.* Generation of ceramide in murine macrophages infected with
697 Leishmania donovani alters macrophage signaling events and aids intracellular
698 parasitic survival. *Mol. Cell. Biochem.* **223**, 47–60 (2001).
699 30. Hamley, J. I. D., Sanchez-Taltavull, D., Koella, J. C. & Stroka, D. Parasitic infection
700 and resource acquisition shape senescence through oxidative stress and energy
701 depletion. *Evol. Int. J. Org. Evol.* **80**, 1905–1916 (2026).
702 31. Xu, F., Song, C., Liu, W. & Chen, G. Protocol for intracellular and extracellular
703 metabolite detection in human embryonic stem cells. *STAR Protoc.* **2**, 100740 (2021).
704 32. Nothias, L.-F. *et al.* Feature-based molecular networking in the GNPS analysis
705 environment. *Nat. Methods* **17**, 905–908 (2020).
706 33. Wang, M. *et al.* Sharing and community curation of mass spectrometry data with
707 Global Natural Products Social Molecular Networking. *Nat. Biotechnol.* **34**, 828–837
708 (2016).
709 34. Kim, H. W. *et al.* NPClassifier: A Deep Neural Network-Based Structural
710 Classification Tool for Natural Products. *J. Nat. Prod.* **84**, 2795–2807 (2021).
711 35. Caporaso, J. G. *et al.* QIIME allows analysis of high-throughput community
712 sequencing data. *Nat. Methods* **7**, 335–336 (2010).

713 36. Vázquez-Baeza, Y., Pirrung, M., Gonzalez, A. & Knight, R. EMPeror: a tool for
714 visualizing high-throughput microbial community data. *Gigascience* **2**, 2047-217X-2–
715 16 (2013).
716 37. Silveira, A. C. A. *et al.* The Trypanosoma cruzi pleiotropic protein P21 orchestrates
717 the intracellular retention and in-vivo parasitism control of virulent Y strain parasites.
718 *Front. Cell. Infect. Microbiol.* **14**, 1412345 (2024).
719 38. Martins, F. A. *et al.* The Recombinant Form of Trypanosoma cruzi P21 Controls
720 Infection by Modulating Host Immune Response. *Front. Immunol.* **11**, 1010 (2020).
721 39. Nogueira, S. S. *et al.* Oxidative stress, cardiomyocytes premature senescence and
722 contractile dysfunction in in vitro and in vivo experimental models of Chagas disease.
723 *Acta Trop.* **244**, 106950 (2023).
724 40. Valieva, Y., Ivanova, E., Fayzullin, A., Kurkov, A. & Igrunkova, A. Senescence-
725 Associated β-Galactosidase Detection in Pathology. *Diagnostics* **12**, 2309 (2022).
726 41. Li, C. *et al.* Resveratrol Prevents Skeletal Muscle Atrophy and Senescence via
727 Regulation of Histone Deacetylase 2 in Cigarette Smoke-Induced Mice with
728 Emphysema. *J. Inflamm. Res.* **15**, 5425–5437 (2022).
729 42. Tang, Y. *et al.* Resveratrol reduces vascular cell senescence through attenuation
730 of oxidative stress by SIRT1/NADPH oxidase-dependent mechanisms. *J. Nutr.*
731 *Biochem.* **23**, 1410–1416 (2012).
732 43. Giovannelli, L. *et al.* Protective Effects of Resveratrol Against Senescence-
733 Associated Changes in Cultured Human Fibroblasts. *J. Gerontol. Ser. A* **66A**, 9–18
734 (2011).

44. Lopes-Paciencia, S. *et al.* The senescence-associated secretory phenotype and its regulation. *Cytokine* **117**, 15–22 (2019).

45. Vilgelm, A. E. *et al.* Connecting the Dots: Therapy-Induced Senescence and a Tumor-Suppressive Immune Microenvironment. *JNCI J. Natl. Cancer Inst.* **108**, (2016).

46. Santana, D. Y. *et al.* MyD88 activation in cardiomyocytes contributes to the heart immune response to acute Trypanosoma cruzi infection with no effect on local parasite control. *PLoS Negl. Trop. Dis.* **12**, e0006617 (2018).

47. Cardoso, M. S., Reis-Cunha, J. L. & Bartholomeu, D. C. Evasion of the Immune Response by Trypanosoma cruzi during Acute Infection. *Front. Immunol.* **6**, (2016).

48. Zhou, T. *et al.* Resveratrol improves osteogenic differentiation of senescent bone mesenchymal stem cells through inhibiting endogenous reactive oxygen species production via AMPK activation. *Redox Rep. Commun. Free Radic. Res.* **24**, 62–69 (2019).

49. Zhou, T. *et al.* Resveratrol improves osteogenic differentiation of senescent bone mesenchymal stem cells through inhibiting endogenous reactive oxygen species production via AMPK activation. *Redox Rep. Commun. Free Radic. Res.* **24**, 62–69 (2019).

50. Zhu, Y. *et al.* The Achilles' heel of senescent cells: from transcriptome to senolytic drugs. *Aging Cell* **14**, 644–658 (2015).

51. Howitz, K. T. *et al.* Small molecule activators of sirtuins extend Saccharomyces cerevisiae lifespan. *Nature* **425**, 191–196 (2003).

52. Baur, J. A. & Sinclair, D. A. Therapeutic potential of resveratrol: the in vivo evidence. *Nat. Rev. Drug Discov.* **5**, 493–506 (2006).

53. Posadino, A. M. *et al.* Flavin Oxidase-Induced ROS Generation Modulates PKC Biphasic Effect of Resveratrol on Endothelial Cell Survival. *Biomolecules* **9**, 209 (2019).

54. Gramatyka, M. Time Does Matter: The Cellular Response to Resveratrol Varies Depending on the Exposure Duration. *Int. J. Mol. Sci.* **26**, 5542 (2025).

55. Bosutti, A. & Degens, H. The impact of resveratrol and hydrogen peroxide on muscle cell plasticity shows a dose-dependent interaction. *Sci. Rep.* **5**, 8093 (2015).

56. Caradonna, K. L., Engel, J. C., Jacobi, D., Lee, C.-H. & Burleigh, B. A. Host Metabolism Regulates Intracellular Growth of Trypanosoma cruzi. *Cell Host Microbe* **13**, 108–117 (2013).

57. De Sá, H. C. *et al.* Alterations in Cardiac Metabolism by *Trypanosoma cruzi* Infection: A Metabolomic Assessment by RPLC-MS and GC–MS. *ACS Infect. Dis.* **11**, 3620–3630 (2025).

58. Dean, D. A. *et al.* Spatial metabolomics identifies localized chemical changes in heart tissue during chronic cardiac Chagas Disease. *PLoS Negl. Trop. Dis.* **15**, e0009819 (2021).

59. Díaz, M. L. *et al.* Metabolomic Profiling of End-Stage Heart Failure Secondary to Chronic Chagas Cardiomyopathy. *Int. J. Mol. Sci.* **23**, 10456 (2022).

60. Knuplez, E. & Marsche, G. An Updated Review of Pro- and Anti-Inflammatory Properties of Plasma Lysophosphatidylcholines in the Vascular System. *Int. J. Mol. Sci.* **21**, 4501 (2020).

61. Venable, M. E., Lee, J. Y., Smyth, M. J., Bielawska, A. & Obeid, L. M. Role of Ceramide in Cellular Senescence. *J. Biol. Chem.* **270**, 30701–30708 (1995).

62. Czibik, G. *et al.* Dysregulated Phenylalanine Catabolism Plays a Key Role in the Trajectory of Cardiac Aging. *Circulation* **144**, 559–574 (2021).

63. Saito, Y. & Chikenji, T. S. Diverse Roles of Cellular Senescence in Skeletal Muscle Inflammation, Regeneration, and Therapeutics. *Front. Pharmacol.* **12**, 739510 (2021).

64. Walle, T., Hsieh, F., DeLegge, M. H., Oatis, J. E. & Walle, U. K. HIGH ABSORPTION BUT VERY LOW BIOAVAILABILITY OF ORAL RESVERATROL IN HUMANS. *Drug Metab. Dispos.* **32**, 1377–1382 (2004).

65. Kapetanovic, I. M., Muzzio, M., Huang, Z., Thompson, T. N. & McCormick, D. L. Pharmacokinetics, oral bioavailability, and metabolic profile of resveratrol and its dimethylether analog, pterostilbene, in rats. *Cancer Chemother. Pharmacol.* **68**, 593–601 (2011).

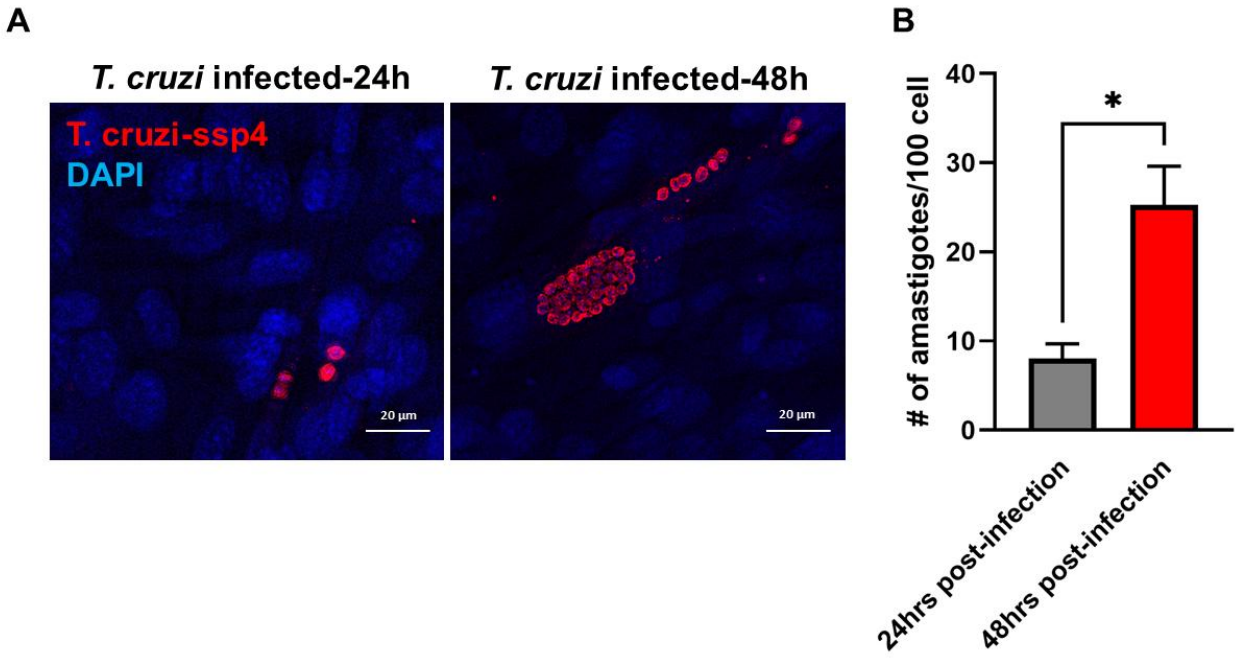

Fig. 1. *T. cruzi* infection model in C2C12 murine myoblasts. (A) Representative immunofluorescence images of C2C12 myoblasts infected with tissue culture-derived *T. cruzi* Brazil strain trypomastigotes at a MOI of 5 at 24 h and 48 h post-infection. Intracellular amastigotes were identified by immunostaining for the stage-specific surface protein SSP4. (B) Quantification of infection rates at 24 and 48 h post-infection. Data represent group means ± standard error of the mean (SEM), n=3. p-value was determined by a two-tailed unpaired t-test (*p<0.05).

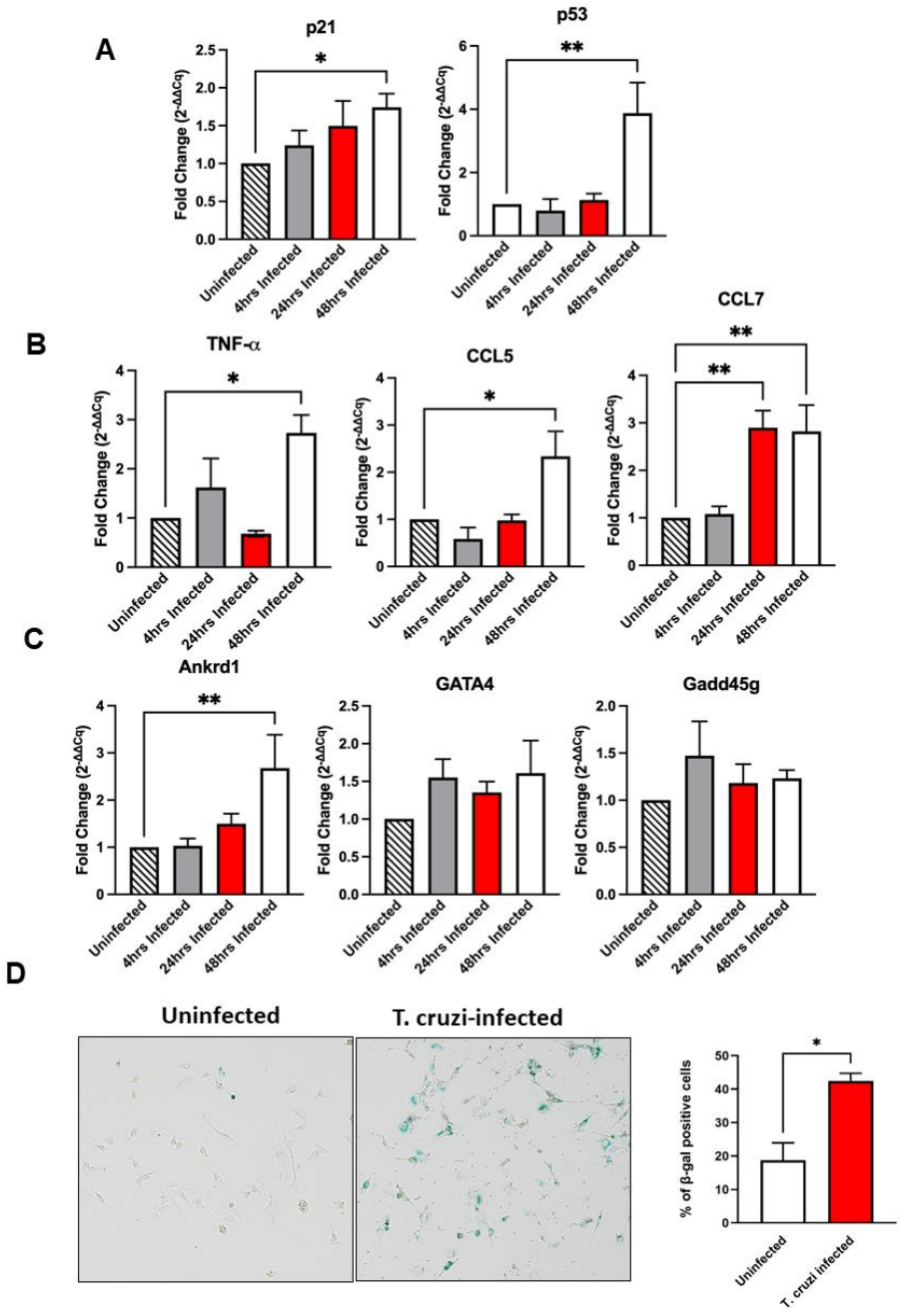

Fig. 2. T. cruzi* infection induces a senescence-like phenotype in host cells.** T. cruzi infection increases expression levels of **(A)** p21 and p53, and **(B)** the inflammatory mediators TNF-α, CCL5 and CCL7. **(C)** *T. cruzi* induces upregulation of Ankrd1, a marker associated with cellular hypertrophy, while GATA4 and Gadd45g show an upward trend following infection. Data represent at least 3 independent experiments. Statistical significance was determined using one-way ANOVA *(p-value< 0.01, *p-value<0.05.* **(D)** Increased SA-β-gal activity following *T.cruzi* infection. p-value was determined by a two-tailed unpaired t-test (*p<0.05), n=3.

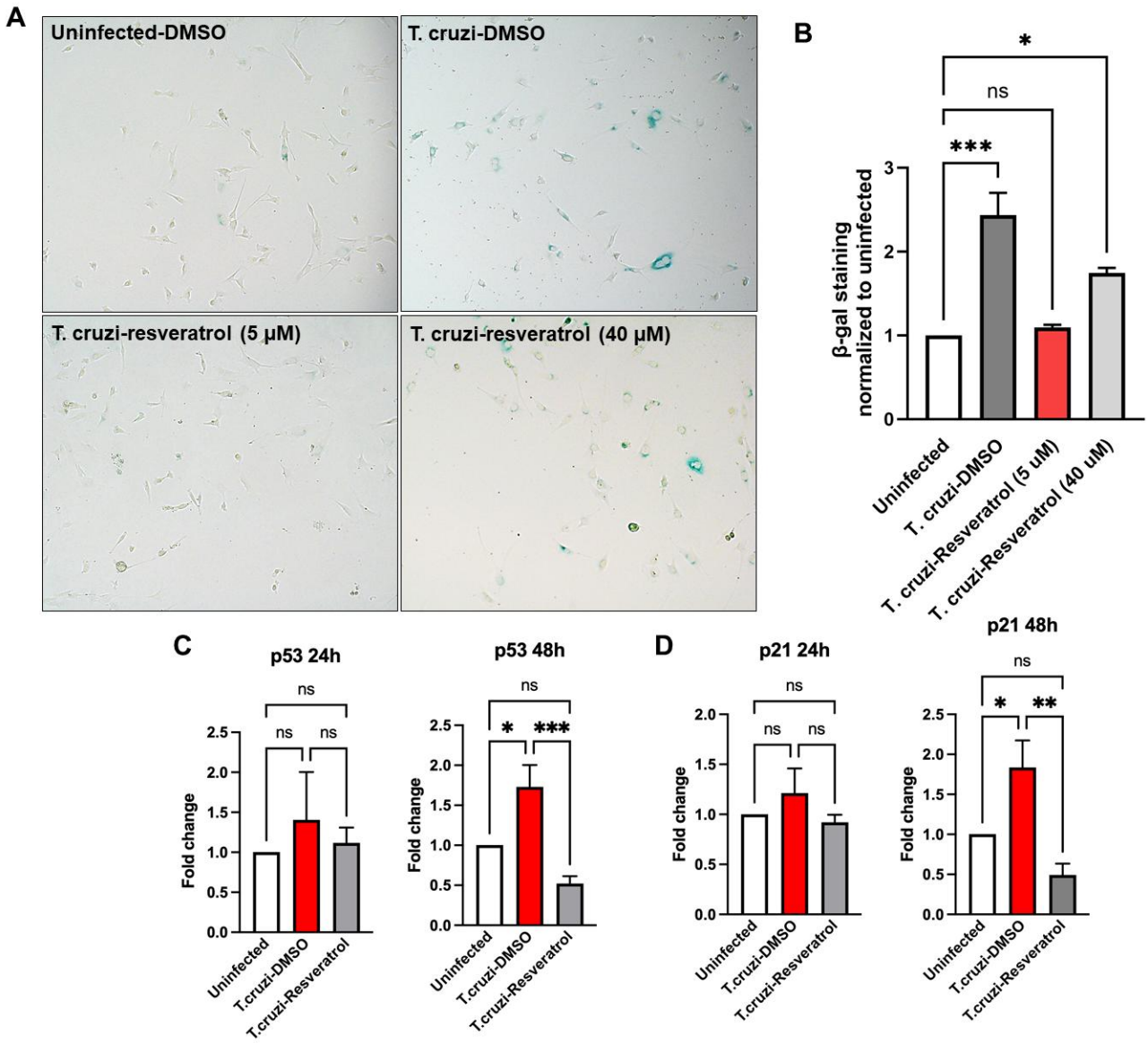

811

812 **Fig. 3. Resveratrol treatment ameliorates *T. cruzi*-induced senescence-like phenotype. (A-B)**
813 Resveratrol treatment at 5 and 40μM significantly reduces the number of senescent cells at 24 h post-
814 infection **(C-D).** 5 μM resveratrol decreases expression levels of p21 and p53 following 48 h post-infection.
815 Data represent at least 3 independent experiments. Statistical analysis was performed using one-way
816 ANOVA (**p-value< 0.01, *p-value<0.05), n=3.

817

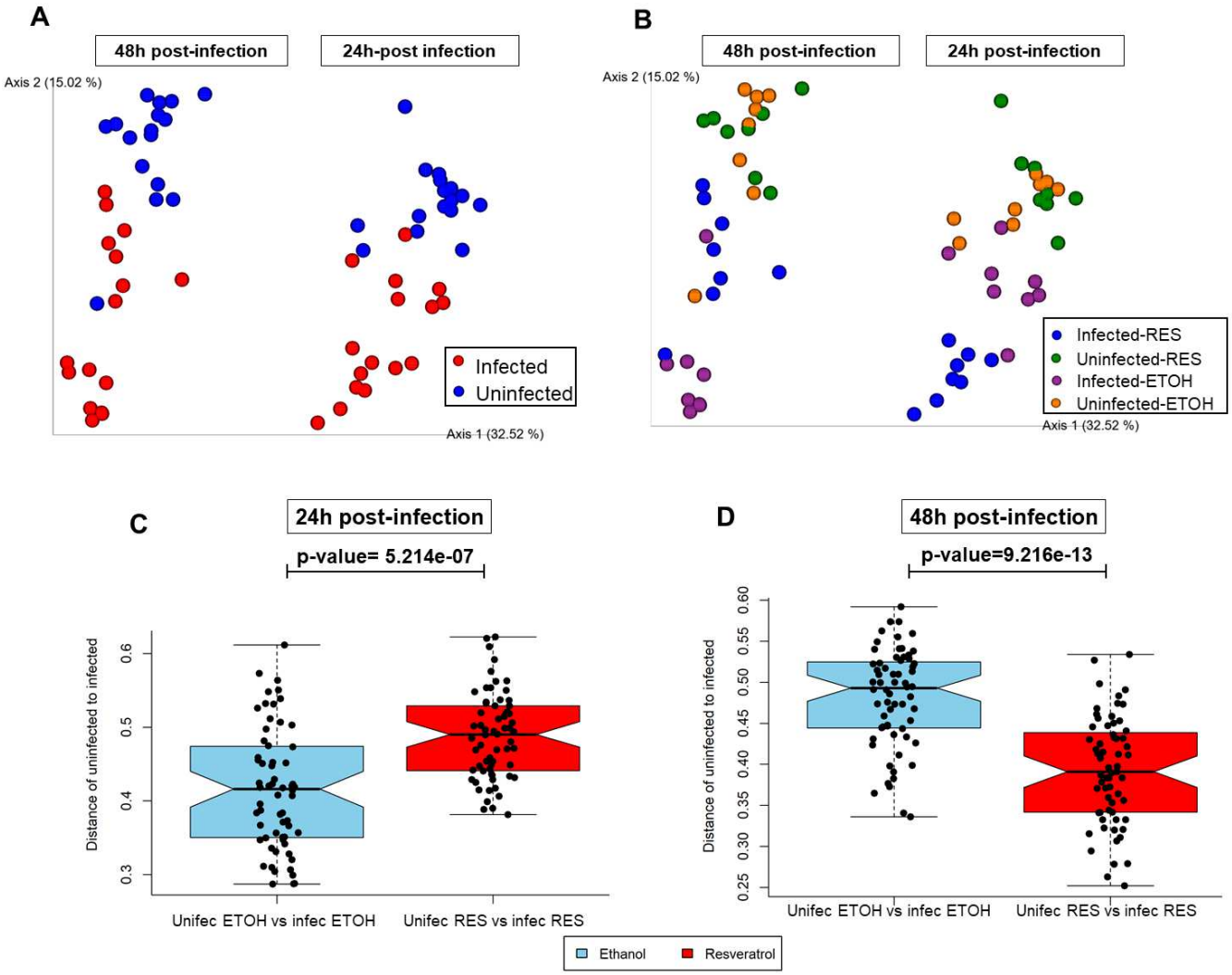

Fig. 4. Resveratrol treatment renormalizes the metabolic profile of intracellular metabolites in *T. cruzi-infected* cells. (A-B) Principal coordinate analysis for intracellular metabolites at 24 h and 48 h timepoints representing infection and treatment groups. **(C-D)** PERMANOVA pseudo-F analysis comparing infected and uninfected groups across treatment and vehicle conditions at 24 and 48 h post-infection. The pseudo-F statistic reflects the degree of separation between infected and uninfected samples at each time point, with higher values indicating greater differences between groups. Statistical significance was assessed using the Wilcoxon rank-sum test. n=8 at each time point.

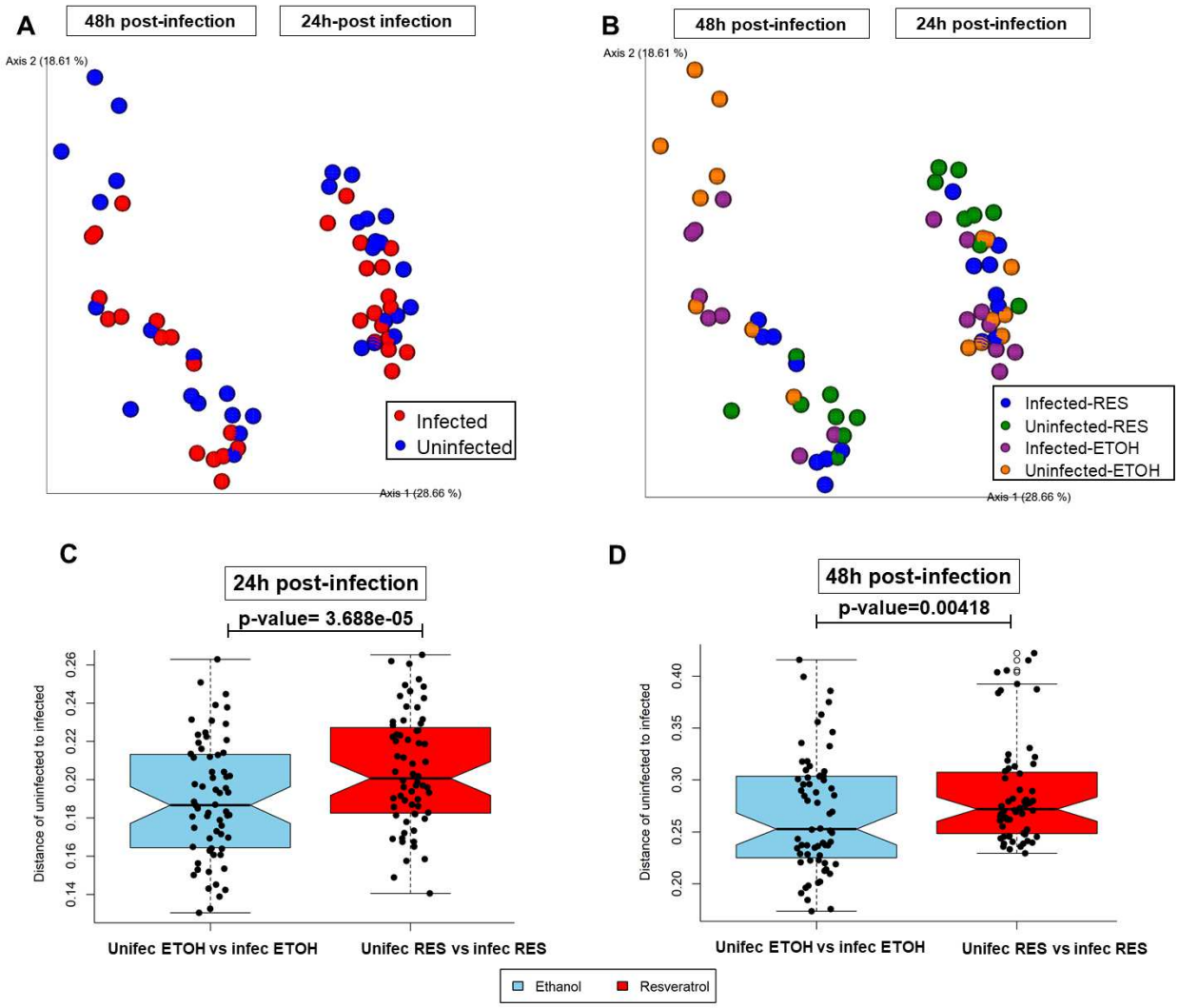

827

828 **Fig. *2*. Resveratrol treatment renormalizes the metabolic profile of extracellular metabolites in *T.***
829 ***cruzi-infected* cells. (A-B)** Principal coordinate analysis for extracellular metabolites at 24 h and 48 h
830 timepoints representing infection and treatment groups. **(C-D)** PERMANOVA pseudo-F analysis comparing
831 infected and uninfected groups across treatment and vehicle conditions at 24 and 48 h post-infection. The
832 pseudo-F statistic reflects the degree of separation between infected and uninfected samples at each time
833 point, with higher values indicating greater differences between groups. Statistical significance was
834 assessed using the Wilcoxon rank-sum test. n=8 at each time point.

835

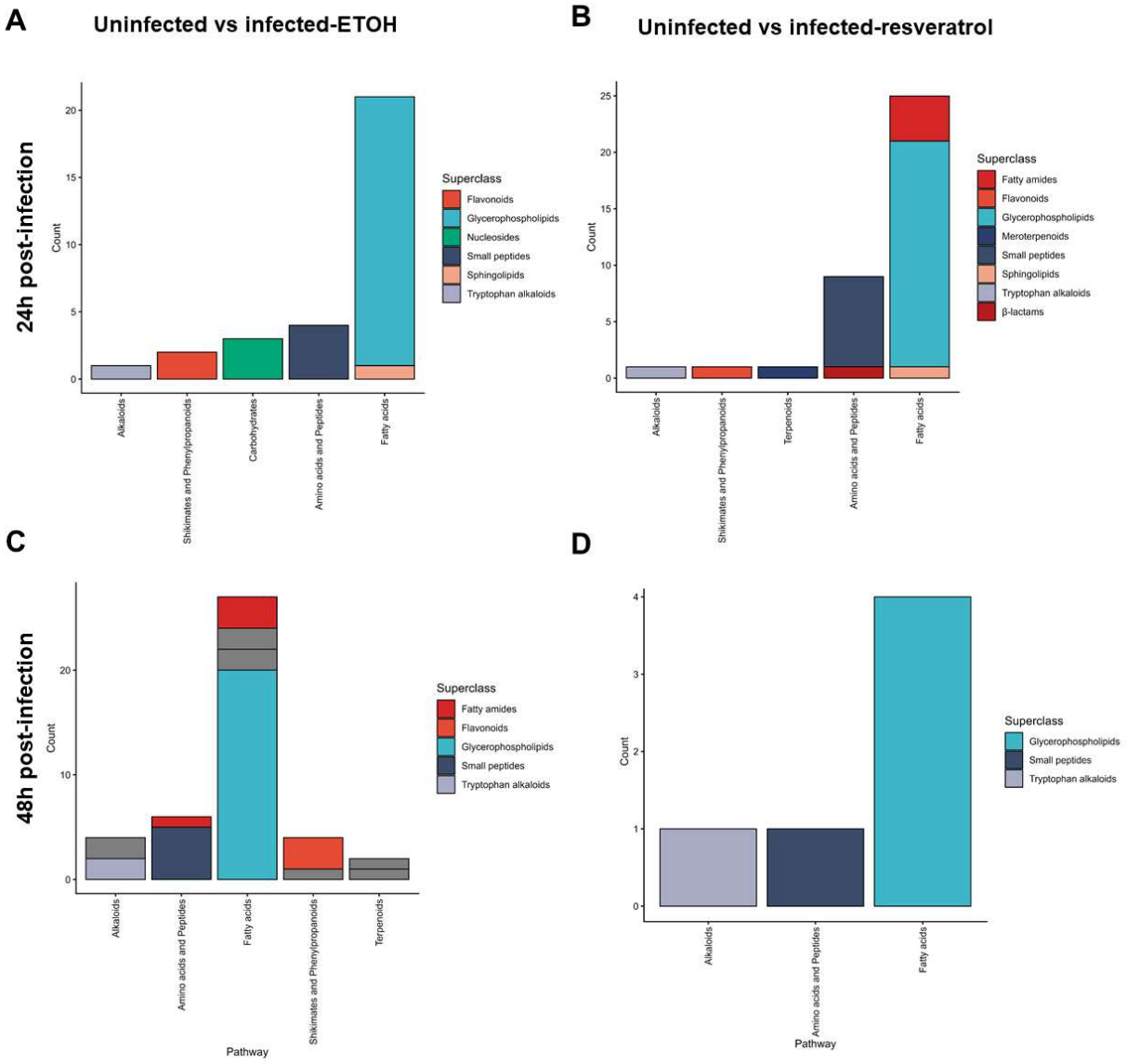

836

837 **Fig.** 3**.** ***T. cruzi*** **infection alters major metabolite families in host cells at 24 h and 48 h post-infection.**
838 Chemical families were assigned using significant metabolites from the comparison of uninfected and
839 infected groups. Available SMILES were used to annotate metabolic families and superclasses using
840 NPClassifier. Data shows metabolites from combined intracellular and extracellular metabolites. **(A, C)**
841 Significantly altered molecular families in *T. cruzi*-infected cells compared with vehicle-treated control cells
842 at 24 and 48 h post-infection, respectively. **(B, D)** Significantly altered molecular families in *T. cruzi*-infected
843 cells treated with resveratrol compared with *T. cruzi*-infected vehicle-treated cells at 24 and 48 h post-
844 infection, respectively.

845

846

847

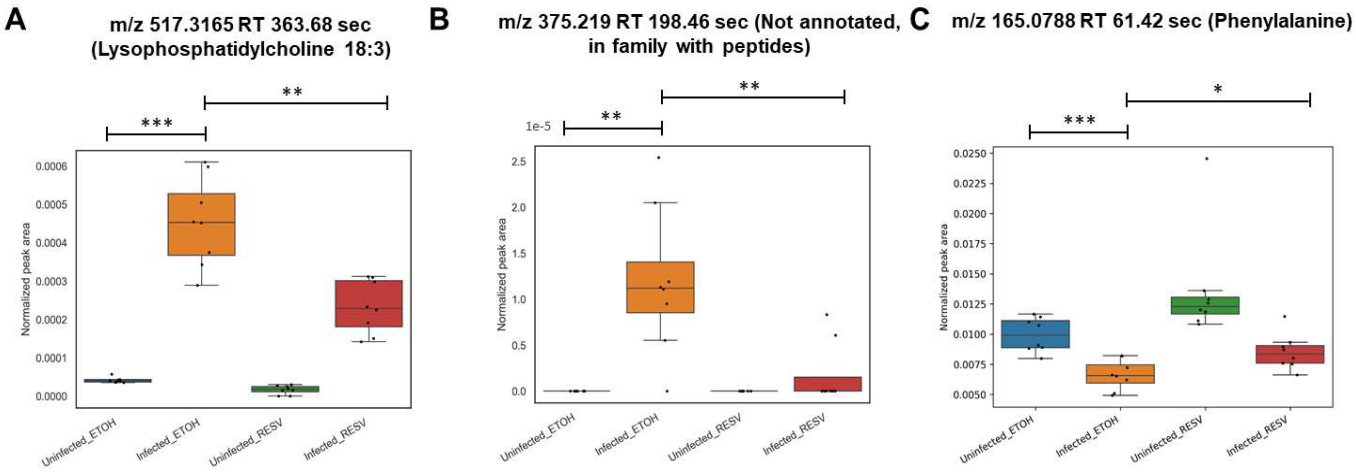

Fig. 7. Resveratrol treatment renormalizes individual metabolites during *T. cruzi* infection. Boxplots comparing the impacts of infection and resveratrol on individual metabolites from **(A-B)** intracellular metabolites at 24 h post-infection and **(C)** an extracellular metabolite at 48 h post-infection. Statistical analysis was performed using the Wilcoxon rank-sum test. (***p-value<0.001, **p-value<0.01, *p-value<0.05), n=8 in each group.

Supplementary Files

This is a list of supplementary files associated with this preprint. Click to download.

- SupplementaryTable3.csv
- SupplementaryTable2.csv
- SupplementaryTable1.csv